GEOLOGY | THE GEOLOGICAL SOCIETY OF AMERICA®

https://doi.org/10.1130/G52255.1

Manuscript received 22 March 2024
Revised manuscript received 3 June 2024
Manuscript accepted 18 June 2024

Published online 12 July 2024

High-precision U-Pb geochronology for the Miocene Climate Optimum and a novel approach for calibrating age models in deep-sea sediment cores

Jennifer Kasbohm[1,2,3,*], Blair Schoene[2], Ellen Thomas[1,4], and Pincelli Hull[1]
[1]Department of Earth & Planetary Sciences, Yale University, New Haven, Connecticut 06511 USA
[2]Department of Geosciences, Princeton University, Princeton, New Jersey 08544, USA
[3]Earth & Planets Laboratory, Carnegie Institution for Science, Washington, D.C. 20015, USA
[4]Department of Earth & Environmental Sciences, Wesleyan University, Middletown, Connecticut 06459, USA

ABSTRACT

Scientific ocean drilling cores recovered years ago (legacy cores), especially as recovered by rotary drilling, commonly show incomplete recovery and core disturbance. We present a novel method to date such cores by presenting the first high-precision U-Pb zircon ages targeting the duration of the Miocene Climate Optimum (MCO; ca. 17–14 Ma) from volcanic ashes at Ocean Drilling Program Site 1000 (on the Nicaragua Rise in the Caribbean Sea). We place these ages within a newly developed framework to address incomplete core recovery and use them to calibrate a high-resolution bulk carbonate $\delta^{13}C$ and $\delta^{18}O$ record. Our Site 1000 ages show that volcanism of the Columbia River Basalt Group (CRBG) large igneous province was coincident with the interval of greatest sustained MCO warmth at this site. However, if the CRBG were the primary driver of the MCO, our chronology may allow for outgassing preceding volcanism as a major source of CO_2. We thus document a promising new way to obtain highly resolved, accurate, and precise numerical age models for legacy deep-sea sediment cores that does not depend on correlation to other records.

INTRODUCTION

Given recent global anthropogenic warming and elevated CO_2 levels, it is important to understand Earth's past warm climates (Steinthorsdottir et al., 2021). The Miocene Climate Optimum (MCO; ca. 17–14 Ma) was marked by global mean surface temperatures 5.3–11.5 °C higher than those of today (e.g., Burls et al., 2021). Various proxies for MCO atmospheric CO_2 suggest concentrations of 400–1000 ppm (Super et al., 2018; Rae et al., 2021; Herbert et al., 2022; Hönisch et al., 2023). The cause of the MCO continues to be debated despite many studies; hypotheses include CO_2 outgassing from large igneous province emplacement of the Columbia River Basalt Group (CRBG; Hodell and Woodruff, 1994), tectonic CO_2 degassing from increased crustal production (Herbert et al., 2022), and changing East Antarctic Ice Sheet dynamics (Foster et al., 2012).

Distinguishing among these hypotheses requires aligning paleoclimatic and paleoceanographic proxy records in numerical time. The stable isotope records defining the MCO have been calibrated primarily by biostratigraphy and/or magnetostratigraphy (with known limitations; e.g., Kasbohm et al., 2021), with fewer records calibrated by astronomical tuning. Astronomical age models currently provide the highest-resolution constraints for paleoceanographic proxy studies; for the Miocene, age constraints can be resolved every 100 k.y. (the short eccentricity cycle; e.g., Holbourn et al., 2007; Kochhann et al., 2016). It remains difficult to test the role of CRBG volcanism in driving the MCO because it has been dated in numerical time using high-precision U-Pb geochronology, which shows that 83% of the eruptive volume of the CRBG was emplaced in ~720 k.y., starting at ca. 16.7 Ma (Kasbohm and Schoene, 2018; Kasbohm et al., 2023). Astronomically tuned age models indicate an onset of MCO warming at 16.9 Ma (Westerhold et al., 2020). The apparent difference in the timing of the onset of warming versus that of volcanism could be due to the different dating methods used.

To date, there are no studies that have used radioisotopic geochronology to construct a timeline for the MCO. This gap in the use of radiometric dating, which can yield highly accurate and precise age models, may be because the most complete MCO records are from deep-sea sediment cores obtained by the International Ocean Discovery Program (IODP) and its predecessors. Such cores yield far smaller samples of volcanic ash layers than are typically used in U-Pb zircon geochronology, and there has been no previous attempt to date IODP cores using zircons from ashes.

We present the first high-precision U-Pb zircon geochronology study of the duration and dynamics of the MCO, with nine dated volcanic ashes in carbonate sediment from Ocean Drilling Program (ODP) Site 1000 (on the Nicaragua Rise in the Caribbean Sea). We use the dates as inputs into Markov Chain Monte Carlo (MCMC) simulations to provide a new age model for the lower-middle Miocene at this site, with 785 bulk carbonate $\delta^{13}C$ and $\delta^{18}O$ measurements across the MCO. Our new age model allows for the first comparison of the time scales of MCO warming and CRBG emplacement using the same chronometer and agrees broadly with astronomically tuned records. We thus show a promising way forward for deriving age models at legacy ocean drill sites—a new priority, given the imminent retirement of the scientific ocean drilling ship, RV *JOIDES Resolution*, with no planned replacement.

Jennifer Kasbohm https://orcid.org/0000-0002-8154-6173
*jkasbohm@carnegiescience.edu

CITATION: Kasbohm, J., et al., 2024, High-precision U-Pb geochronology for the Miocene Climate Optimum and a novel approach for calibrating age models in deep-sea sediment cores: Geology, v. XX, p. , https://doi.org/10.1130/G52255.1

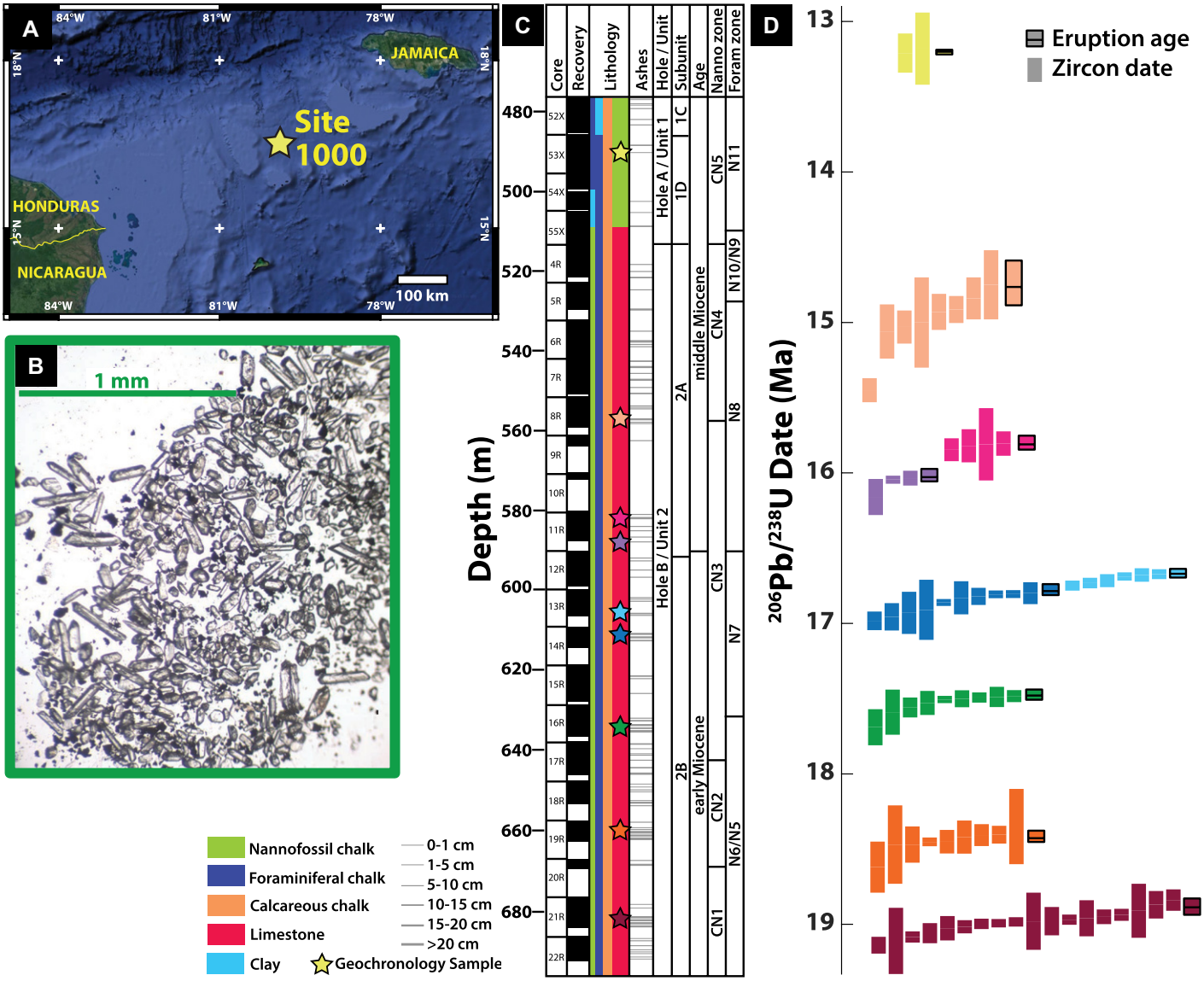

Figure 1. (A) Map of Ocean Drilling Program (ODP) Site 1000 on the Nicaragua Rise in the Caribbean Sea (16°33.223'N, 79°52.044'W; satellite imagery from Google Earth™). Yellow line is the boundary between Honduras and Nicaragua. (B) Zircon yield from volcanic ash from sample 1000B-16R4. (C) Simplified stratigraphic column for the lower to middle Miocene at ODP Site 1000 (Shipboard Scientific Party, 1997a). Dominant to minor lithologies are depicted from right to left. Nanno—calcareous nannofossil; Foram—planktonic foraminifera. (D) Rank order plot of $^{206}Pb/^{238}U$ dates. Each bar represents a date for a single zircon, with the length of the bar showing 2σ analytical uncertainty. Analyses for each sample are grouped by color, highlighting the results of our Bayesian zircon eruptive age modeling (Keller et al., 2018) (median and 95% credible interval) that are input into our Markov Chain Monte Carlo (MCMC) superposition age model.

SITE, SAMPLES, AND METHODS

Our study required locating a deep-sea coring site with both MCO-aged carbonates and volcanic ashes with sufficient zircons for robust U-Pb dates. ODP Site 1000 (16°33.223'N, 79°52.044'W, 916 m water depth, drilled in 1996; Fig. 1) met these criteria (based on shipboard biostratigraphy; Shipboard Scientific Party, 1997a). This site has numerous ash beds due to its proximity to prolonged silicic volcanic activity in the Central American arc (Carey and Sigurdsson, 2000). Megascopic ash layers comprise >1% of Site 1000's total cored volume, with 161 layers totaling 826 cm thickness (Shipboard Scientific Party, 1997a). The felsic mineral assemblage of these tephras includes minerals that commonly co-occur with zircon, such as quartz, biotite, and hornblende. $^{40}Ar/^{39}Ar$ geochronology had been attempted on some ashes, but reported ages were imprecise and out of stratigraphic order (Sigurdsson et al., 2000), thus of little use to construct an age model.

We received 15 ash samples from 488.69 m to 683.46 m below seafloor (mbsf; ca. 19–13.5 Ma based on shipboard age models of Cande and Kent, 1995, and Berggren et al., 1995), nine of which yielded zircons. When samples exhibited low zircon yield, all grains available were analyzed. Individual zircons were separated from each sample and dated through chemical abrasion–isotope dilution–thermal ionization mass spectrometry (CA-ID-TIMS) at Princeton University (USA; see the Supplemental Material[1] for methods). 785 bulk carbonate (chalk and limestone) samples were pulverized and analyzed for $\delta^{13}C$ and $\delta^{18}O$ at the Yale Analytical and Stable Isotope Center (Yale University, USA; see the Supplemental Material).

Our studied interval at ODP Site 1000 was rotary cored (Shipboard Scientific Party, 1997a). Recovery was incomplete, averaging

[1]Supplemental Material. Materials, methods, and data (Tables S1–S4). Please visit https://doi.org/10.1130/GEOL.S.26072686 to access the supplemental material; contact editing@geosociety.org with any questions.

68.7% for cores 1000B-4R through 1000B-22R and ranging from 15%–105% for individual cores. Cores were drilled over ~10 m intervals, so that the depth of each core is constrained within that interval, but the true depth of sediment intervals (thus samples) within each cored interval is uncertain due to drilling disturbance and incomplete recovery. By convention, depths are assigned to recovered sediment as if all recovered material came from the top of the cored interval (Shipboard Scientific Party, 1997b), but this convention does not necessarily reflect the original depth-location of recovered and missing sediment. Rotary drilling disturbs, and poorly recovers, soft sediments interbedded with relatively hard sediments (chalks, limestones); soft sediments may be flushed away by drilling mud. To account for uncertainty in the actual original distribution of recovered sediments, we assigned depths to sediments by two approaches in addition to the convention (the first approach) (see the Supplemental Material). We preferred the second approach, which assumed that recovered sediment fragments were originally distributed evenly across the 10 m depth span of each core. The third approach assigned all recovered sediments to the lowest part of the core. We constructed age models for each of these three depth schemas and show the distributed model outputs here (other models are provided in the Supplemental Material).

RESULTS

Because zircons may crystallize over a prolonged time period prior to the eruption of a magma chamber (Simon et al., 2008; Cooper, 2015), individual zircon dates within each sample spread beyond analytical uncertainty (95% confidence intervals shown; Fig. 1D). These dispersed zircon dates were input into a MCMC model, using all dates and uncertainties, with priors for the distribution of zircon crystallization prior to eruption informed by time, temperature, and melt fraction, to provide an estimate of the eruption age for each ash bed (Keller et al., 2018). Eruption ages were input into a second MCMC simulation (Schoene et al., 2019) that uses samples' stratigraphic order to further refine these ages (Fig. 2A; Table S2 in the Supplemental Material). Using the second MCMC model, we calculated sedimentation rates for the studied interval (25–40 m/m.y.; Fig. 2B). These models were used to assign numerical ages to our stable isotope measurements (Fig. 3; Table S3) and available biostratigraphic data for ODP Site 1000 (Table 1). The credible intervals shown for our model ages represent only analytical uncertainty; systematic uncertainties are provided in the Supplemental Material. The three approaches used to approximate the downhole depth of the samples do not substantially offset ash or biostratigraphy ages. Calculated ages for stable isotope measurements are more sensitive to depth uncertainties reflected by poorly recovered intervals (Fig. 3; Fig. S7). The magnitude of

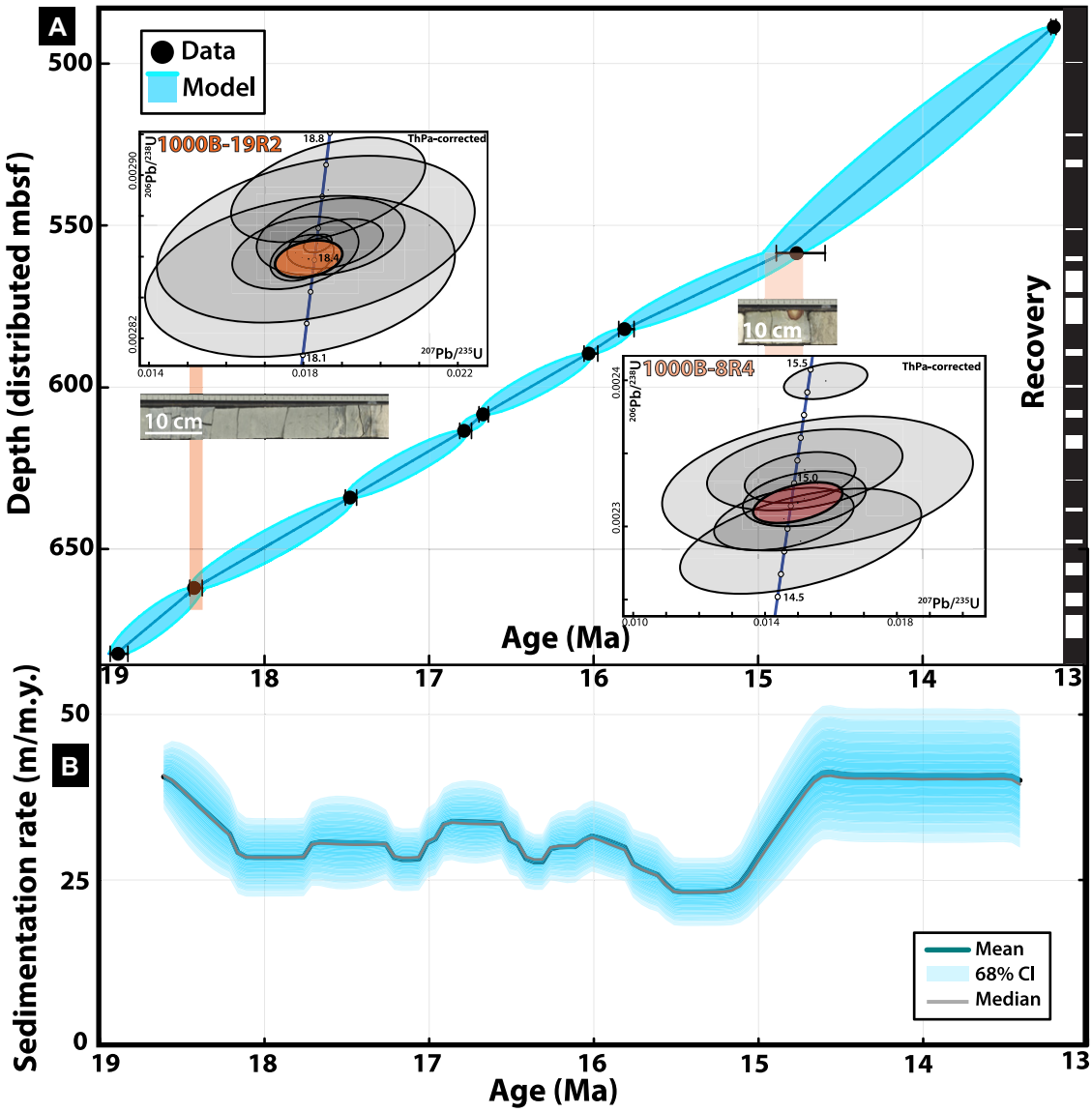

Figure 2. (A) U-Pb age-depth Markov Chain Monte Carlo (MCMC) superposition model results, with shading indicating 95% credible intervals, two representative Concordia plots of Ocean Drilling Program (ODP) Site 1000 samples from the Nicaragua Rise in the Caribbean Sea), ash images, and schematic recovery. ThPa—thorium and protactinium; mbsf—meters below sea floor. (B) Results from A were used in further MCMC simulation to calculate sedimentation rates, averaged over 500 k.y. windows, shown with contours up to the 68% credible interval.

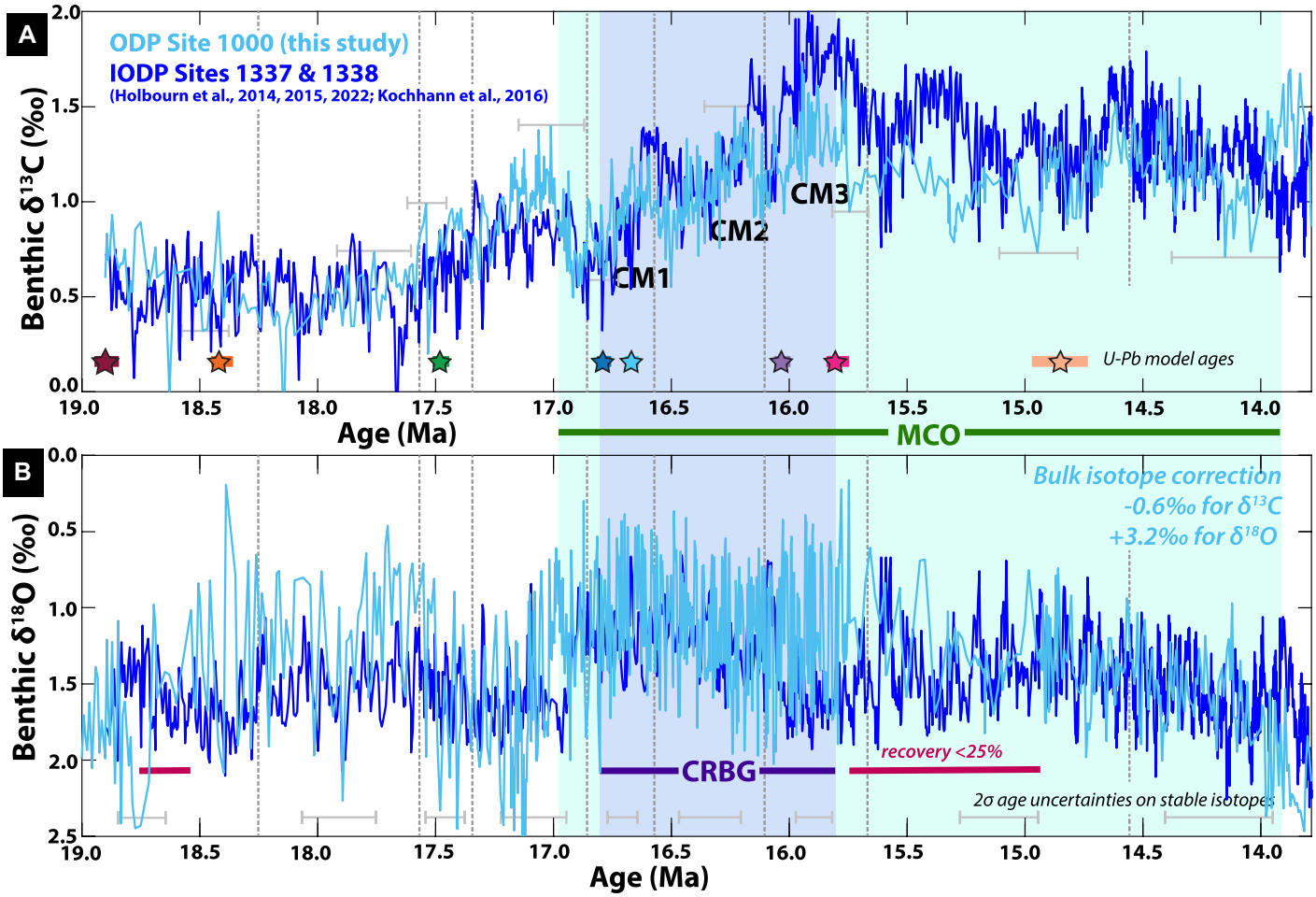

Figure 3. $\delta^{13}C$ (A) and $\delta^{18}O$ (B) bulk isotopes from Ocean Drilling Program (ODP) Site 1000 (on the Nicaragua Rise in the Caribbean Sea), corrected to allow comparison of benthic isotopes from International Ocean Discovery Program (IODP) Sites U1337 and U1338 in the eastern Equatorial Pacific Ocean. Model ages for geochronology samples are starred, with 95% credible intervals. Gray bars indicate average 95% credible intervals in the ages modeled for each stable isotope measurement in time ranges bracketed by dotted lines, which represent change points in average uncertainties across our studied interval. MCO—Miocene Climate Optimum; CRBG—Columbia River Basalt Group.

TABLE 1. AGE MODEL RESULTS FOR MIOCENE BIOSTRATIGRAPHIC DATA PREVIOUSLY REPORTED FOR OCEAN DRILLING PROGRAM SITE 1000

Shipboard Scientific Party (1997a); Kameo and Bralower (2000)						This study				GTS 2020
Type	Species	Event	Depth (mbsf)	Age (Ma)	References	Distributed Depth (mbsf)	Age (Ma)	+2σ (Ma)	−2σ (Ma)	Age (Ma)
CN	*Cyclicargolithus floridanus*	T	498.35	13.19	Raffi and Flores (1995)	498.35	13.431	0.169	0.146	13.33
CN	*Sphenolithus heteromorphus*	T	514.00	13.57	Raffi and Flores (1995)	514.18	13.804	0.230	0.220	13.6
CN	*Helicosphera ampliaperta*	T	557.35	15.83	Backman et al (1990)	559.05	14.867	0.125	0.120	14.86
CN	*Sphenolithus heteromorphus*	B	642.30	18.1	Olafsson (1991)	643.17	17.786	0.169	0.158	17.65
CN	*Sphenolithus belemnos*	T	642.30	18.4	Olafsson (1991)	643.17	17.786	0.169	0.158	17.94
CN	*Sphenolithus belemnos*	B	668.90	19.7	Olafsson (1991)	673.75	18.698	0.124	0.129	19.01
PF	*Fohsella praefohsi*	FO	510.00	14.0		510.00	13.705	0.218	0.205	13.77
PF	*Fohsella peripheroacuta*	FO	527.60	14.8		529.38	14.161	0.234	0.235	14.06
PF	*Orbulina suturalis*	FO	527.60	15.1		529.38	14.161	0.234	0.235	15.12
PF	*Praeorbulina circularis*	FO	537.15	16.0	Berggren et al. (1995); Cande and Kent (1995)	537.15	14.344	0.222	0.229	15.98
PF	*Praeorbulina glomerosa*	FO	546.75	16.1		547.21	14.581	0.189	0.201	16.27
PF	*Praeorbulina sicana*	FO	590.05	16.4		590.10	16.050	0.062	0.049	16.39
PF	*Catapsydrax dissimilis*	LO	633.40	17.3		633.86	17.473	0.038	0.056	17.54

Note: Table data are from Kameo and Bralower (2000) and Shipboard Scientific Party (1997a, calibrated to time scales referenced therein) and compared to those data reported in the Geologic Time Scale (GTS) 2020 (Raffi et al., 2020). CN—calcareous nannofossils; PF—planktonic foraminifera; T—top of species range (last appearance datum); B—bottom of species range (first appearance datum); FO—first occurrence; LO—last occurrence; mbsf—meters below sea floor; green—agreement between ages from this study and 2020; yellow—ages from this study within 100 ka of GTS 2020/poor core recovery; pink—offset between this study and GTS 2020.

age uncertainty for our isotopic measurements decreases with increased density of dated ashes, especially for cores with high recovery (Fig. 3). We used a change point analysis of uncertainties in our stable isotope ages to see how uncertainty varied through time (Fig. 3). To compare our bulk carbonate records from Site 1000, where the signal is primarily sourced from calcareous nannofossils and planktonic foraminifera (Mutti et al., 2005), with MCO records derived from benthic foraminifera (Fig. 3), we shifted values by −0.6‰ for $\delta^{13}C$ and +3.2‰ for $\delta^{18}O$.

DISCUSSION

Our work represents not only the first time that U-Pb CA-ID-TIMS zircon geochronology has been used to constrain the timing of onset and duration of the MCO, but also the first time this technique has been applied to volcanic ashes

from deep-sea sediment cores. U-Pb geochronology has been used to date igneous intrusion samples from the deep sea (Eddy et al., 2017), but sample size constraints may have prevented it from being applied to thin ashes interbedded in sediments. Directly dating zircons in ashes from deep sea cores may provide a new way to anchor astrochronological age models (used throughout paleoclimatology) in numerical time. Furthermore, we robustly quantify the uncertainty of our age model, which is rarely done for deep-sea sediment cores. Dating ashes could improve age models at sites where drilling disturbances, core recovery, and/or poor preservation prevent the development of astrochronology.

We compared our results to those of Eastern Equatorial Pacific Integrated Ocean Drilling Program (IODP) Sites U1337 (3°50.009′N, 123°12.352′W) and U1338 (2°30.469′N, 117°58.178′W) (Holbourn et al., 2014, 2015, 2022; Kochhann et al., 2016), which are key astrochronology reference sites for the early and middle Miocene (Fig. 3). Our U-Pb age model for MCO bulk isotopes at ODP Site 1000 agrees well with these MCO benthic isotope records. Compared to benthic isotope records, bulk isotopes are much more susceptible to the effects of diagenesis and variability in microfossil assemblages, though bulk and benthic isotope records may vary coherently (e.g., Reghellin et al., 2020). We identified carbon isotope maxima (CM) events 1–3 at Site 1000 and see excellent overall alignment between $\delta^{13}C$ records at IODP Sites U1337 and U1338 and ODP Site 1000. For $\delta^{18}O$, we see general agreement in the shape of the curves, though our bulk isotope record is, as expected, marked by higher amplitude variability. Low $\delta^{18}O$ values indicate the MCO onset and continuation after 17 Ma, but the hyperthermal event at 15.6 Ma identified at Site U1338 was not observed at Site 1000. Poor recovery (15%–20%) and diagenesis could account for the missed event. One key difference in the bulk $\delta^{18}O$ records at Site 1000 and the benthic records at other sites is in the apparent timing of the MCO onset, at ca. 16.9 Ma at Site U1337 and at ca. 17.1 Ma at Site 1000, but this is within the error of ages modeled for the MCO onset (Fig. 3). Aligning the Site 1000 $\delta^{18}O$ record to a 16.9 Ma warming onset would worsen the agreement between bulk and benthic $\delta^{13}C$ records, so we suggest caution in interpreting bulk $\delta^{18}O$ data (Reghellin et al., 2020). The apparent difference in timing of the onset of warming might be due to diagenesis, poor preservation, or reflect a locally/regionally diachronous onset of the MCO.

We can now revisit the role of the CRBG in driving MCO warming as observed at ODP Site 1000, as both the isotope events and CRBG are dated with the same geochronometer and MCMC age modeling. The $\delta^{18}O$ records at Site 1000 reaffirm that CRBG main-phase volcanism (ca. 16.7–15.9 Ma) was coincident with the MCO interval of greatest sustained warmth (Kasbohm et al., 2023). However, the onset of the MCO, in both the astronomically tuned record from IODP Site U1337 and, possibly, our U-Pb-calibrated record from Site 1000, preceded the onset of CRBG extrusive volcanism by a few hundred thousand years. Voluminous sub-surface CRBG sill emplacement may have released an enormous quantity of CO_2 a few hundred thousand years prior to CRBG volcanism (Tian and Buck, 2022), a possible mechanism to produce MCO warming prior to surface eruptions and consistent with our observations. We speculate that outgassing associated with CRBG emplacement could have contributed to MCO warmth, but we cannot be certain of the primary cause of the warming.

Our ODP Site 1000 oxygen isotopes exhibit low values from 18.5 Ma to 17.5 Ma, which may indicate warming prior to the MCO. Elevated MCO temperatures and Antarctic deglaciation may have been preconditioned by a prolonged interval of early Miocene global warmth starting at 18.5 Ma (Drury et al., 2021). The timing of this warm interval may coincide with a major extinction in sharks at ca. 19 Ma and a notable paucity of lower Miocene sediments in ocean drilling archives (Sibert and Rubin, 2021). While many Miocene climate studies have focused on the MCO, these findings, together with our data, highlight the need to better understand the early Miocene.

Finally, our age model suggests refined age estimates with uncertainty for ODP Site 1000 biostratigraphic data (Shipboard Scientific Party, 1997a; Kameo and Bralower, 2000) compared to ages in the Geologic Time Scale (GTS) 2020 (Raffi et al., 2020), though we recommend the biostratigraphy of Site 1000 be revisited given our new age model. Our calculated ages for calcareous nannofossil events mostly agree with GTS 2020 (Table 1), though we find the base of *Sphenolithus belemnos* at ca. 18.7 Ma rather than 19.01 Ma. This later onset may be due to poor core recovery (25%) or locally delayed appearance. Poor preservation may also explain the later onsets for planktonic foraminifera markers *Orbulina suturalis*, *Praeorbulina circularis*, *P. glomerosa*, and *P. sicana* at Site 1000. As yet, we do not suggest revisions to GTS 2020, but our approach of dating zircons in deep-sea ashes could yield robust age constraints in better-preserved cores in the future.

OUTLOOK

We provide a radioisotopic age model for the MCO by a novel application of U-Pb CA-ID-TIMS geochronology to ashes in deep-sea sediments (ODP Site 1000). We provide numerical ages with robust quantification of uncertainty, thereby showing a promising way to date cores (if they have ashes with zircons) that may be hard to otherwise age-calibrate. In future work, zircon ages could be used to anchor relative markers and age models in numerical time. The imminent cessation of operations of RV *JOIDES Resolution* will lead to a protracted hiatus in the scientific acquisition of long, deep-sea sediment cores, if not the end of ocean drilling as we know it. It is therefore imperative to investigate legacy cores with new methodologies, as geologic time is the ultimate variable required to interpret paleoclimate proxy data.

ACKNOWLEDGMENTS

This research used samples and data provided by the Ocean Drilling Program (ODP) and made use of the Yale Analytical and Stable Isotope Center at Yale University (Connecticut, USA); we thank B. Erkkila. We thank A. Holbourn for helpful conversations, D. Suwondo for logistical support, and T. Westerhold and I. Raffi for constructive reviews. This material is based upon work supported by the National Science Foundation under award no. 1952753.

REFERENCES CITED

Berggren, W.A., Kent, D.V., Swisher, C.C., and Aubry, M., 1995, A revised Cenozoic geochronology and chronostratigraphy, *in* Berggren, W.A., et al., eds., Geochronology, Time Scales and Global Stratigraphic Correlation: Society for Sedimentary Geology (SEPM), v. 54, https://doi.org/10.2110/pec.95.04.0129.

Burls, N.J., et al., 2021, Simulating Miocene warmth: Insights from an opportunistic multi-model ensemble (MioMIP1): Paleoceanography and Paleoclimatology, v. 36, https://doi.org/10.1029/2020PA004054.

Cande, S.C., and Kent, D.V., 1995, Revised calibration of the geomagnetic polarity timescale for the Late Cretaceous and Cenozoic: Journal of Geophysical Research: Solid Earth, v. 100, p. 6093–6095, https://doi.org/10.1029/94JB03098.

Carey, S., and Sigurdsson, H., 2000, Grain size of Miocene volcanic ash layers from Sites 998, 999, and 1000: Implications for source areas and dispersal, *in* Leckie, R.M., et al., eds., Proceedings of the Ocean Drilling Program, Scientific Results, v. 165: College Station, Texas, Ocean Drilling Program, p. 101–113, https://doi.org/10.2973/odp.proc.sr.165.002.2000.

Cooper, K.M., 2015, Timescales of crustal magma reservoir processes: Insights from U-series crystal ages, *in* Caricchi, L., and Blundy, J.D., eds., Chemical, Physical and Temporal Evolution of Magmatic Systems: Geological Society, London, Special Publication 422, p. 141–174, https://doi.org/10.1144/SP422.7.

Drury, A.J., et al., 2021, Climate, cryosphere and carbon cycle controls on Southeast Atlantic orbital-scale carbonate deposition since the Oligocene (30–0 Ma): Climate of the Past, v. 17, p. 2091–2117, https://doi.org/10.5194/cp-17-2091-2021.

Eddy, M.P., Jagoutz, O., and Ibañez-Mejia, M., 2017, Timing of initial seafloor spreading in the Newfoundland-Iberia rift: Geology, v. 45, p. 527–530, https://doi.org/10.1130/G38766.1.

Foster, G.L., Lear, C.H., and Rae, J.W.B., 2012, The evolution of pCO_2, ice volume and climate during the middle Miocene: Earth and Planetary Science Letters, v. 341–344, p. 243–254, https://doi.org/10.1016/j.epsl.2012.06.007.

Herbert, T.D., Dalton, C.A., Liu, Z., Salazar, A., Si, W., and Wilson, D.S., 2022, Tectonic degassing drove global temperature trends since 20 Ma: Science, v. 377, p. 116–119, https://doi.org/10.1126/science.abl4353.

Hodell, D.A., and Woodruff, F., 1994, Variations in the strontium isotopic ratio of seawater during the Miocene: Stratigraphic and geochemical implications: Paleoceanography, v. 9, p. 405–426, https://doi.org/10.1029/94PA00292.

Holbourn, A., Kuhnt, W., Schulz, M., Flores, J.A., and Andersen, N., 2007, Orbitally-paced climate evolution during the middle Miocene "Monterey" carbon-isotope excursion: Earth and Planetary Science Letters, v. 261, p. 534–550, https://doi.org/10.1016/j.epsl.2007.07.026.

Holbourn, A., Kuhnt, W., Lyle, M., Schneider, L., Romero, O., and Andersen, N., 2014, Middle Miocene climate cooling linked to intensification of eastern equatorial Pacific upwelling: Geology, v. 42, p. 19–22, https://doi.org/10.1130/G34890.1.

Holbourn, A., Kuhnt, W., Kochhann, K.G.D., Andersen, N., and Sebastian Meier, K.J., 2015, Global perturbation of the carbon cycle at the onset of the Miocene Climatic Optimum: Geology, v. 43, p. 123–126, https://doi.org/10.1130/G36317.1.

Holbourn, A., Kuhnt, W., Kochhann, K.G.D., Matsuzaki, K.M., and Andersen, N., 2022, Middle Miocene climate–carbon cycle dynamics: Keys for understanding future trends on a warmer Earth? *in* Aiello, I.W., Barron, J.A., and Ravelo, A.C., eds., Understanding the Monterey Formation and Similar Biosiliceous Units across Space and Time: Geological Society of America Special Paper 556, p. 93–111, https://doi.org/10.1130/2022.2556(05).

Hönisch, B., et al., 2023, Toward a Cenozoic history of atmospheric CO_2: Science, v. 382, https://doi.org/10.1126/science.adi5177.

Kameo, K., and Bralower, T.J., 2000, Neogene calcareous nannofossil biostratigraphy of Sites 998, 999, and 1000, Caribbean Sea, *in* Leckie, R.M., et al., eds., Proceedings of the Ocean Drilling Program, Scientific Results, v. 165: College Station, Texas, Ocean Drilling Program, p. 3–15, https://doi.org/10.2973/odp.proc.sr.165.012.2000.

Kasbohm, J.J., and Schoene, B., 2018, Rapid eruption of the Columbia River flood basalt and correlation with the mid-Miocene climate optimum: Science Advances, v. 4, https://doi.org/10.1126/sciadv.aat8223.

Kasbohm, J., Schoene, B., Montanari, A., and Coccioni, R., 2021, High-precision U–Pb zircon geochronology of the Miocene Bisciaro Formation, Contessa Section, Italy: A case study for requisite radioisotopic calibration of bio- and magnetostratigraphy: Palaeogeography, Palaeoclimatology, Palaeoecology, v. 576, https://doi.org/10.1016/j.palaeo.2021.110487.

Kasbohm, J., Schoene, B., Mark, D.F., Murray, J., Reidel, S., Szymanowski, D., Barfod, D., and Barry, T., 2023, Eruption history of the Columbia River Basalt Group constrained by high-precision U-Pb and $^{40}Ar/^{39}Ar$ geochronology: Earth and Planetary Science Letters, v. 617, https://doi.org/10.1016/j.epsl.2023.118269.

Keller, C.B., Schoene, B., and Samperton, K.M., 2018, A stochastic sampling approach to zircon eruption age interpretation: Geochemical Perspectives Letters, v. 8, p. 31–35, https://doi.org/10.7185/geochemlet.1826.

Kochhann, K.G.D., Holbourn, A., Kuhnt, W., Channell, J.E.T., Lyle, M., Shackford, J.K., Wilkens, R.H., and Andersen, N., 2016, Eccentricity pacing of eastern equatorial Pacific carbonate dissolution cycles during the Miocene Climatic Optimum: Paleoceanography, v. 31, p. 1176–1192, https://doi.org/10.1002/2016PA002988.

Mutti, M., Droxler, A.W., and Cunningham, A.D., 2005, Evolution of the Northern Nicaragua Rise during the Oligocene–Miocene: Drowning by environmental factors: Sedimentary Geology, v. 175, p. 237–258, https://doi.org/10.1016/j.sedgeo.2004.12.028.

Rae, J.W.B., Zhang, Y.G., Liu, X., Foster, G.L., Stoll, H.M., and Whiteford, R.D.M., 2021, Atmospheric CO_2 over the past 66 million years from marine archives: Annual Review of Earth and Planetary Sciences, v. 49, p. 609–641, https://doi.org/10.1146/annurev-earth-082420-063026.

Raffi, I., Wade, B.S., and Pälike, H., 2020, The Neogene Period, *in* Gradstein, F.M., et al., eds., Geologic Time Scale 2020: Amsterdam, Elsevier, v. 2, p. 1141–1215, https://doi.org/10.1016/B978-0-12-824360-2.00029-2.

Reghellin, D., Dickens, G.R., Coxall, H.K., and Backman, J., 2020, Understanding bulk sediment stable isotope records in the eastern Equatorial Pacific, from seven million years ago to present day: Paleoceanography and Paleoclimatology, v. 35, https://doi.org/10.1029/2019PA003586.

Schoene, B., Eddy, M.P., Samperton, K.M., Keller, C.B., Keller, G., Adatte, T., and Khadri, S.F.R., 2019, U-Pb constraints on pulsed eruption of the Deccan Traps across the end-Cretaceous mass extinction: Science, v. 363, p. 862–866, https://doi.org/10.1126/science.aau2422.

Shipboard Scientific Party, 1997a, Site 1000, *in* Sigurdsson, H., et al., eds., Proceedings of the Ocean Drilling Program, Initial Reports, v. 165: College Station, Texas, Ocean Drilling Program, p. 231–289, https://doi.org/10.2973/odp.proc.ir.165.105.1997.

Shipboard Scientific Party, 1997b, Explanatory Notes, *in* Sigurdsson, H., et al., eds., Proceedings of the Ocean Drilling Program, Initial Reports, v. 165: College Station, Texas, Ocean Drilling Program, p. 15–46, https://doi.org/10.2973/odp.proc.ir.165.102.1997.

Sibert, E.C., and Rubin, L.D., 2021, An early Miocene extinction in pelagic sharks: Science, v. 372, p. 1105–1107, https://doi.org/10.1126/science.aaz3549.

Sigurdsson, H., Kelley, S.P., Leckie, R.M., Carey, S., Bralower, T.J., and King, J., 2000, History of circum-Caribbean explosive volcanism: $^{40}Ar/^{39}Ar$ dating of tephra layers, *in* Sigurdsson, H., et al., eds., Proceedings of the Ocean Drilling Program, Scientific Results, v. 165: College Station, Texas, Ocean Drilling Program, p. 299–314, https://doi.org/10.2973/odp.proc.sr.165.021.2000.

Simon, J.I., Renne, P.R., and Mundil, R., 2008, Implications of pre-eruptive magmatic histories of zircons for U-Pb geochronology of silicic extrusions: Earth and Planetary Science Letters, v. 266, p. 182–194, https://doi.org/10.1016/j.epsl.2007.11.014.

Steinthorsdottir, M., et al., 2021, The Miocene: The Future of the Past: Paleoceanography and Paleoclimatology, v. 36, https://doi.org/10.1029/2020PA004037.

Super, J.R., Thomas, E., Pagani, M., Huber, M., O'Brien, C., and Hull, P.M., 2018, North Atlantic temperature and pCO_2 coupling in the early-middle Miocene: Geology, v. 46, p. 519–522, https://doi.org/10.1130/G40228.1.

Tian, X., and Buck, W.R., 2022, Intrusions induce global warming before continental flood basalt volcanism: Nature Geoscience, v. 15, p. 417–422, https://doi.org/10.1038/s41561-022-00939-w; erratum available at https://doi.org/10.1038/s41561-022-01005-1.

Westerhold, T., et al., 2020, An astronomically dated record of Earth's climate and its predictability over the last 66 million years: Science, v. 369, p. 1383–1387, https://doi.org/10.1126/science.aba6853.

Printed in the USA